AGU PUBLICATIONS

Geophysical Research Letters

RESEARCH LETTER
10.1002/2017GL075375

Key Points:
- Surface temperature should be compared with downward infrared radiation and not net infrared radiation
- The Arctic surface temperature trend is driven primarily by downward infrared radiation and not surface turbulent fluxes
- The downward infrared radiation trend is associated with the intraseasonal moisture intrusion trend

Correspondence to:
S. Lee,
sxl31@psu.edu

Citation:
Lee, S., Gong, T., Feldstein, S. B., Screen, J. A., & Simmonds, I. (2017). Revisiting the cause of the 1989–2009 Arctic surface warming using the surface energy budget: Downward infrared radiation dominates the surface fluxes. *Geophysical Research Letters*, *44*, 10,654–10,661. https://doi.org/10.1002/2017GL075375

Received 25 APR 2017
Accepted 6 OCT 2017
Accepted article online 11 OCT 2017
Published online 28 OCT 2017

Revisiting the Cause of the 1989–2009 Arctic Surface Warming Using the Surface Energy Budget: Downward Infrared Radiation Dominates the Surface Fluxes

Sukyoung Lee[1], Tingting Gong[2], Steven B. Feldstein[1], James A. Screen[3], and Ian Simmonds[4]

[1]Department of Meteorology and Atmospheric Science, Pennsylvania State University, University Park, PA, USA, [2]Key Laboratory of Ocean Circulation and Waves, Institute of Oceanology, Chinese Academy of Sciences and Qingdao National Laboratory for Marine Science and Technology, Qingdao, China, [3]Department of Mathematics, University of Exeter, Exeter, Devon, UK, [4]School of Earth Sciences, University of Melbourne, Parkville, VIC, Australia

Abstract The Arctic has been warming faster than elsewhere, especially during the cold season. According to the leading theory, ice-albedo feedback warms the Arctic Ocean during the summer, and the heat gained by the ocean is released during the winter, causing the cold-season warming. Screen and Simmonds (2010; SS10) concluded that the theory is correct by comparing trend patterns in surface air temperature (SAT), surface turbulence heat flux (HF), and net surface infrared radiation (IR). However, in this comparison, downward IR is more appropriate to use. By analyzing the same data used in SS10 using the surface energy budget, it is shown here that over most of the Arctic the skin temperature trend, which closely resembles the SAT trend, is largely accounted for by the downward IR, not the HF, trend.

Plain Language Summary The Arctic has been warming faster than elsewhere, especially during the fall and winter. According to the leading theory, ice-albedo feedback warms the Arctic Ocean during the summer, and the heat gained by the ocean is released during the fall and winter, causing warming in these seasons. Deviating from this theory, it is shown here that over most of the Arctic, the skin temperature trend, which closely resembles the SAT trend, is largely accounted for by the downward infrared radiation, not the ocean-to-atmosphere heat flux, trend.

1. Introduction

Over the past several decades, the Arctic has been warming more rapidly than other parts of the Earth. This warming is particularly strong during winter. Climate model simulations also show that Arctic amplification is stronger during winter (e.g., Serreze & Francis, 2006). The viewpoint of the leading theory on this topic is that when sea ice area declines during the summer (due to greenhouse gas warming), the ice-albedo feedback mechanism causes more heat to be deposited into the ocean. According to this scenario, this warming of the ocean during the summer hinders the subsequent cold-season growth of sea ice (e.g., Serreze et al., 2009; Screen & Simmonds, 2010a; Serreze & Barry, 2011; Stroeve et al., 2012) and results in a warming of the overlying atmosphere due to an upward flux of the heat deposited in the ocean.

Screen and Simmonds (2010b) (SS10 hereafter) set out to test this hypothesis using ERA-Interim data. They examined the October–January mean 1989–2009 trends in surface air temperature (SAT), sea ice concentration, surface net infrared radiation (IR), and surface sensible and latent heat fluxes. The surface net IR was defined as downward IR minus upward IR. They found that surface heat flux trend pattern matches reasonably well with the SAT trend pattern and that the surface net IR trend pattern is weak and does not match with the SAT trend pattern. Based on these findings, they conclude that the IR effect does not play a dominant role and, consistent with the above hypothesis, they conclude that the main cause of the upward SAT trend is the increased upward surface heat flux. The need to discuss this paper was brought to the attention of the first three authors of this paper in the review process of their earlier work (Gong et al., 2017), where they conclude, also with ERA-Interim data, that the December–February mean Arctic SAT warming trend during the 1991–2010 period can be accounted for mostly by the downward IR trend, with the surface heat flux playing a limited and local role in Arctic amplification. Because this topic is at the heart of the rapid Arctic climate change, we feel that it would be beneficial to reconcile the difference in the conclusions of the two studies by carefully comparing the findings of SS10 to those in Gong et al. (2017), but using the same data over the identical time period as in SS10.

The SAT is a commonly used variable in climate studies, yet it is the skin temperature, T_s, which can be readily interpreted in terms of surface energy balance. Following equation (1) of Lesins et al. (2012), but including the storage term $G \left(= \int_0^{\delta z} \rho c_p \left(\frac{dT_s}{dt}\right) dz\right)$, where δz is the thickness of a thin interface, and the other variables are standard, the surface energy budget may be written as

$$G = S_d + S_u + I_d + I_u + F_{\mathrm{sh}} + F_{\mathrm{lh}} + R, \tag{1}$$

where S and I are shortwave and longwave radiation and the subscript d denotes downward and u upward. F_{sh} is the surface sensible heat flux, F_{lh} is surface latent heat flux, and the residual R includes heat conduction through sea ice, heat loss (gain) through the melting (freezing) of sea ice, and over the open ocean, R also includes the turbulent heat flux due to mixing in the ocean boundary layer and horizontal heat flux convergence associated with ocean currents. The atmospheric energy fluxes are defined as positive if they are directed downward (toward the interface), while R is defined positive if the conduction/flux is directed upward (again toward the interface). The interface can be understood as encompassing a very thin layer of air above the surface and a very thin layer of soil, water, snow, or sea ice below the surface. For the atmospheric part of this thin layer, it can be seen as corresponding to the very thin layer above the surface (a few millimeters thick) where heat transport by molecular conduction is stronger than that by turbulent heat fluxes (Wallace & Hobbs, 2006). It is important to note that a typical storage layer extends downward to a depth where the temperature undergoes little change. Therefore, the temperature in a typical storage layer differs from T_s. However, because the storage layer is infinitesimally thin, the average temperature will be extremely close to T_s. Furthermore, because the storage layer includes air and soil, water, snow, or sea ice, to be more precise, ρ and $c_p$in G should include values across the interface.

Taking the differential of both sides in (1), where the differential operator Δ represents the trend, and neglecting the shortwave flux for the winter season, the equation for the trend in the surface energy budget can be written as

$$\Delta G = \Delta I_d + \Delta I_u + \Delta F_{\mathrm{sh}} + \Delta F_{\mathrm{lh}} + \Delta R. \tag{2}$$

The storage term G is vanishingly small because an infinitesimally thin (δz being very small) air surface interface has a very small heat capacity (Lesins et al., 2012). Therefore, ΔT_s comes into (2) from the radiative cooling term, that is, I_u. Expressing I_u as $-\varepsilon\sigma {T_s}^4$ (a minus sign because it is upward) where σ is the Stefan-Boltzmann constant and ε is the surface emissivity, and taking its differential, equation (2) can be rewritten as

$$\Delta T_s = (\Delta I_d + \Delta F_{\mathrm{sh}} + \Delta F_{\mathrm{lh}} + \Delta R) / \left(4\varepsilon\sigma {T_s}^3\right), \tag{3}$$

where the storage term G has been dropped. Equation (3) tells us that a trend in T_s is associated with trends in downward IR (ΔI_d), ΔF_{sh}, ΔF_{lh}, and ΔR. Equation (3) indicates that the trend in T_s (or the trend in the SAT; the daily SAT and T_s are very highly correlated (Chen et al., 2002); $r = 0.97$) should be compared with the trend in downward IR. The energy budget terms in (3) can be readily computed using available data sets such as ERA-Interim reanalysis.

In comparison, it is challenging to compute the energy budget in terms of the SAT. In this case, one must consider the radiative and heat flux *convergences* into a thin atmospheric layer centered at 2 m above the ground. For the IR radiation, the time rate of change in the SAT is proportional to the sum of the upward energy flux at the bottom of the layer minus the upward energy flux at the top of the layer and the downward energy flux at the top of the layer minus the downward energy flux at the bottom of the layer. Neglecting shortwave radiation (for Arctic winter), the flux convergence is then

$$\left(I_{U,B} - I_{U,T}\right) + \left(I_{D,T} - I_{D,B}\right) + \left(F_B - F_T\right), \tag{4}$$

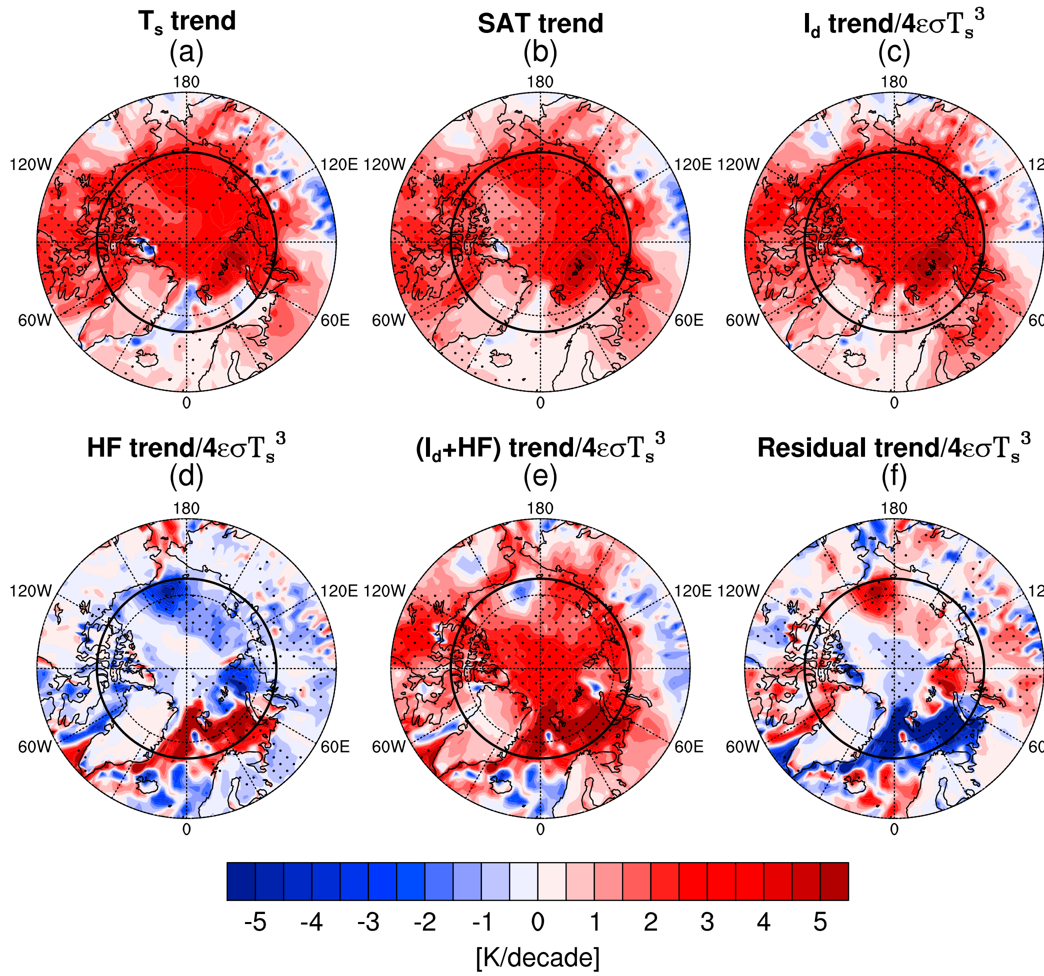

Figure 1. The 1989–2009 October–January linear trends (°K/decade) of (a) the skin temperature T_s, (b) the SAT, (c) the downward IR divided by $4\varepsilon\sigma T_s^3$, (d) the surface heat flux divided by $4\varepsilon\sigma T_s^3$, (e) the summation of the downward IR and surface heat flux divided by $4\varepsilon\sigma T_s^3$, and (f) the residual (see the text for more detail). The dots show values that are statistically significant at the $p < 0.10$ level for a Student's t test.

where $I_{U,B}$ is upward IR, $I_{D,B}$ is downward IR, and F_B is the sum of the sensible and latent turbulent energy fluxes at the *bottom* of the layer; $I_{U,T}$ is upward IR, $I_{D,T}$ is downward IR, and F_T is the sum of the sensible and latent turbulent energy fluxes at the *top* of the layer. These energy budget terms are much more difficult to evaluate than the surface energy budget terms. In SS10, an explicit energy balance equation was not used. However, in Figure 2 of SS10, they do compare $\Delta(I_d - I_u)$ and $\Delta(F_{sh} + F_{lh})$, which are terms in the surface energy balance. Because the bottom of the layer at 2 m faces the surface, if we assume that $I_{D,B} = I_d$, $I_{U,B} = I_u$, and $F_B = F_{sh} + F_{lh}$, then the comparison between $\Delta(I_d - I_u)$ and $\Delta(F_{sh} + F_{lh})$ amounts to a comparison between $\Delta(I_{D,B} - I_{U,B})$ and ΔF_B. As we can see from (3) and (4), it is incorrect to consider the net surface IR as the IR forcing term even for the SAT.

Although the daily SAT and T_s are highly correlated, for longer time scales, it is possible that the correlation is smaller, especially over regions with a strongly stratified boundary layer. However, as we show in Figures 1a and 1b, over most of the Arctic, ΔT_s and ΔSAT remain comparable in their pattern and magnitude. (In the ERA-Interim data set, T_s is calculated from the surface energy balance (https://www.ecmwf.int/en/about; ECMWF Part IV, Physical Processes.) A notable exception is found over the Greenland Sea and the southern part of Barents Sea where $\Delta(\text{SAT} - T_s)$ is slightly positive (not shown). These regions are mostly ice free, and as will be revisited in section 3, the cooling trend in T_s is likely caused by turbulence flux in the ocean mixed layer. Given the overall agreement between ΔT_s and ΔSAT, we evaluate the terms in (3) and attempt to reconcile the conclusion of SS10 and that of Gong et al. (2017).

2. Data and Methods

In this study, we compute the energy budget terms in (3) using the same data source (ERA-Interim data) for the same months (October–January) and time period (1989–2009) as SS10. For the surface and radiative fluxes, daily accumulated values at time steps 3 and 6 for 00:00 UTC and 12:00 UTC are used. For each UTC, the fluxes are obtained by computing the difference between the step 6 and step 3 forecasted values and by dividing this difference by the time interval in seconds. The resulting 00:00 UTC and 12:00 UTC forecasted flux averages are then averaged to obtain the daily surface and radiative flux values. The ERA-Interim does not provide the heat conduction term, *C*. Therefore, this term is omitted in our analysis.

3. Results

3.1. The Budget Analysis

Figures 1c–1e, respectively, show $\Delta I_d/4\varepsilon\sigma T_s^{\,3}$, $(\Delta F_{\mathrm{sh}} + \Delta F_{\mathrm{lh}})/4\varepsilon\sigma T_s^{\,3}$, and $(\Delta I_d + \Delta F_{\mathrm{sh}} + \Delta F_{\mathrm{lh}})/4\varepsilon\sigma T_s^{\,3}$. The surface emissivity ε is set to 1, and at each grid point the October–January mean values averaged over the 21 year period are used for T_s in the denominator. Because ε is in the denominator of the right-hand side of (3), the relative importance of the various surface flux terms does not depend on its specific value. By comparing Figures 1c–1e with Figure 1a, it is evident that the downward IR term, $\Delta I_d/4\varepsilon\sigma T_s^{\,3}$, is the largest term on the right-hand side of (3). The trends in Figures 1a and 1c are positive over virtually all regions in the Arctic.

The surface heat flux trend in Figure 1d, $(\Delta F_{\mathrm{sh}} + \Delta F_{\mathrm{lh}})/4\varepsilon\sigma T_s^{\,3}$, is more complex: there are positive trends over the Greenland Sea (although statistical significance is marginal in this region) and over most of the Barents Sea, indicating trends of anomalous atmosphere-to-surface heat fluxes in this region. This particular region is masked in Figures 2c–2e of SS10 by gray shading. (Although not mentioned in SS10, the intention of the masking was to focus on ice-covered regions.) Therefore, a comparison with SS10 cannot be made for this region. Over other parts of the Arctic Ocean, the flux trend is negative, i.e., a surface heat flux trend from the surface to the atmosphere. This trend field (Figure 1d) compares very well with Figure 2e of SS10. (Note that their sign convention for the surface heat flux is opposite to ours. In SS10, positive values indicate an upward flux.) SS10 concluded that the upward surface heat flux is the dominant driver of the SAT. However, over those parts of the Arctic where the surface heat flux trend is negative, i.e., an upward heat flux trend, with the exception of small parts of the Chukchi and Kara Seas, Figure 1e shows that the magnitude of the surface heat flux trend is smaller than that of the downward IR trend. Therefore, the results of our analysis are at odds with the conclusions of SS10 and indicate that the downward IR is the dominant, not a minor, contributor to the winter SAT and skin temperature increase.

The sum of the downward IR and surface heat flux trends, i.e., $(\Delta I_d + \Delta F_{\mathrm{sh}} + \Delta F_{\mathrm{lh}})/4\varepsilon\sigma T_s^{\,3}$ (Figure 1e), shows a close match with the skin temperature trend, i.e., ΔT_s (Figure 1a), over most of the Arctic. Those regions where these trends differ can be identified by subtracting $(\Delta I_d + \Delta F_{\mathrm{sh}} + \Delta F_{\mathrm{lh}})/4\varepsilon\sigma T_s^{\,3}$ from ΔT_s (Figure 1f). This difference between these two trends is the residual, i.e., $\Delta R/(4\varepsilon\sigma T_s^{\,3})$ in (3). As can be seen, the residual is largest over the Greenland, southern Barents, and Chukchi Seas. During the winter season, the Greenland and southern Barents Seas lack sea ice coverage, whereas the Chukchi and the northern part of the Barents and Kara Seas are mostly ice covered, although as shown in SS10, it is these seas that underwent the largest decline in sea ice. As discussed above, over the ice-covered parts of the Arctic Ocean, $\Delta R/(4\varepsilon\sigma T_s^{\,3})$ can correspond to the trend in conduction of heat through the sea ice. On the other hand, for open water, $\Delta R/(4\varepsilon\sigma T_s^{\,3})$ corresponds to a trend in the turbulent vertical heat flux due to mixing in the ocean, in addition to horizontal heat transport trend by ocean currents. The largest values of the residual in Figure 1f are consistent with a thinning of sea ice over the Chukchi Sea and therefore an increase in upward heat conduction. For the Greenland and southern Barents Seas, it is consistent with a downward turbulent heat flux from the ocean surface into the mixed layer, which offsets the warming of the ocean surface due to the positive trend in both the downward IR (Figure 1c) and downward surface heat fluxes (Figure 1d). In regions of perennial sea ice cover over the central Arctic, the residual has a weak but statistically significant negative trend, indicating less heat conduction through the ice. This is consistent with an increase of the skin temperature (Figure 1a) because a decreasing temperature gradient between the ice surface and ice bottom will lead to less upward heat conduction.

3.2. A Cause of the Downward IR Trend

Given the results of the above budget analysis, a natural question to ask is what causes the downward IR to increase. Gong et al. (2017) and others showed that the intraseasonal midlatitude winter circulation is an

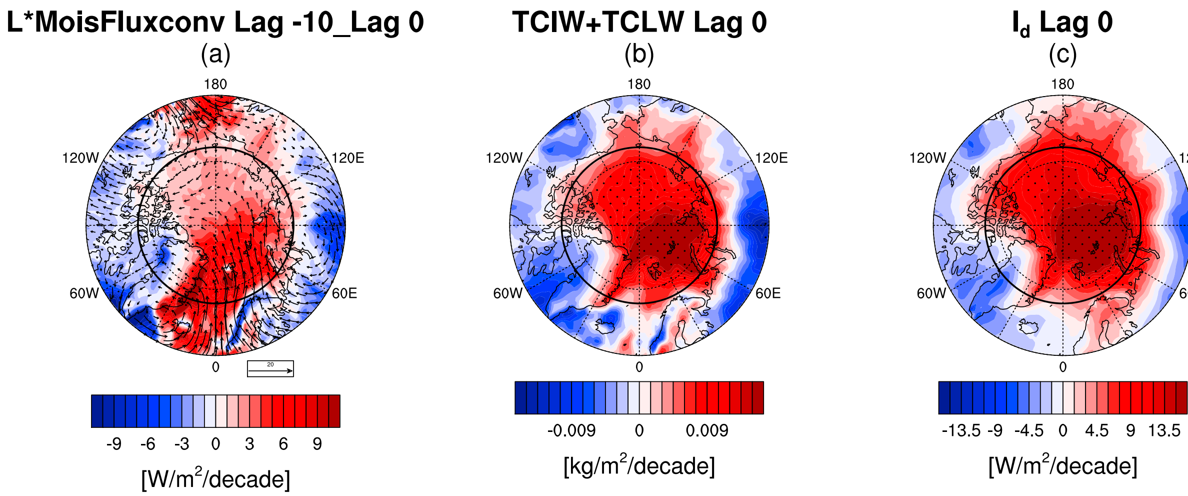

Figure 2. The trends for selected moist thermodynamic variables obtained by multiplying the regression coefficients (regression against the IR index) and the trend in the IR index. Trends are shown for the vertically integrated moisture flux vectors and moisture flux convergence multiplied by the latent heat of (a) vaporization, L (L*MoisFluxconv), (b) total column condensed water (liquid water plus ice) (TCIW + TCLW), and (c) the downward IR (downward IR). The lag chosen for TCIW + TCLW and downward IR is lag 0 days and the average of the lag day −10 through lag day 0 trends for the moisture flux. The dots indicate values that are statistically significant at the $p < 0.10$ level for a Student's t test.

important contributor to the downward IR increase on the same time scale (Baggett et al., 2016; Doyle et al., 2011; Lee et al., 2011; Luo et al., 2017; Park, Lee, & Feldstein, 2015; Park, Lee, Son, et al., 2015; Woods et al., 2013; Woods & Caballero, 2016; Yoo et al., 2012a, 2012b). Doyle et al. (2011) analyzed in situ data in the high Arctic and speculated that increases in warm moist air intrusions into the Arctic could contribute to long-term warming over the Arctic. Lee et al. (2011) showed that more frequent occurrences of particular intraseasonal teleconnections have contributed to long-term Arctic warming through their impact on downward IR. Yoo et al. (2011) showed that the more frequent occurrence of a certain phase of the Madden-Julian Oscillation contributed to the Arctic warming. Along the same lines, Park, Lee, and Feldstein (2015), Woods and Caballero (2016), and Gong et al. (2017) showed that a long-term increase in the intraseasonal moisture intrusions into the Arctic can help account for the positive trend in the downward IR during the winter season over recent decades. Gong and Luo (2017) showed that more frequent Ural blocking is associated with the sea ice decline in the Barents-Kara Seas. Therefore, we test if the above process occurs for the same data as in SS10.

To examine if a similar process is involved for the trends in the present study, as in Park, Lee, and Feldstein (2015) and Gong et al. (2017), we construct a daily IR index by projecting the daily downward IR field onto the interdecadal (1989–2009) downward IR linear trend pattern in Figure 1b. The projection domain is poleward of 70°N. (The 70°N latitude is indicated by the thick circle in all of the figures presented in this study.) With this downward IR trend projection time series, which we denote as x, one can obtain an associated trend of any variable, y, at any grid point. The linear trend of y associated with the trend of x, $\Delta_x y$, can be written as

$$\Delta_x y(\tau) = [r(\tau)\sigma(y)/\sigma(x)]\Delta x \tag{5}$$

where Δx is the 1989–2009 linear trend in x,$r(\tau)$ is the linear correlation between the *daily* values of $x(t)$ and $y(t+\tau)$ for time lag τ, and $\sigma(x)$ and $\sigma(y)$ are the standard deviations of x and y, respectively. In (4), the quantity $r(\tau)\sigma(y)/\sigma(x)$ is the lagged regression coefficient. For our calculation of $r(\tau)$, as in Gong et al. (2017), the October–December mean values of x and y are subtracted for each year. Equation (5) was constructed from the perspective that the intraseasonal relationship between x and y, in combination with the trend in x, contributes to the linear trend in y. We also consider time lags to examine the lag-lead relationship between x and y. We denote the trend of y associated with the linear trend of x as $\Delta_x y$ to distinguish it from its linear trend, Δy. In particular, it needs to be recognized that the downward IR trend associated with x, $\Delta_x I_d$, can be different from its own linear trend ΔI_d.

Consistent with the findings by Park, Lee, and Feldstein (2015) and Gong et al. (2017), we see that within the 10 day interval leading up to local peak in x, there is an enhanced moisture flux convergence (multiplied by

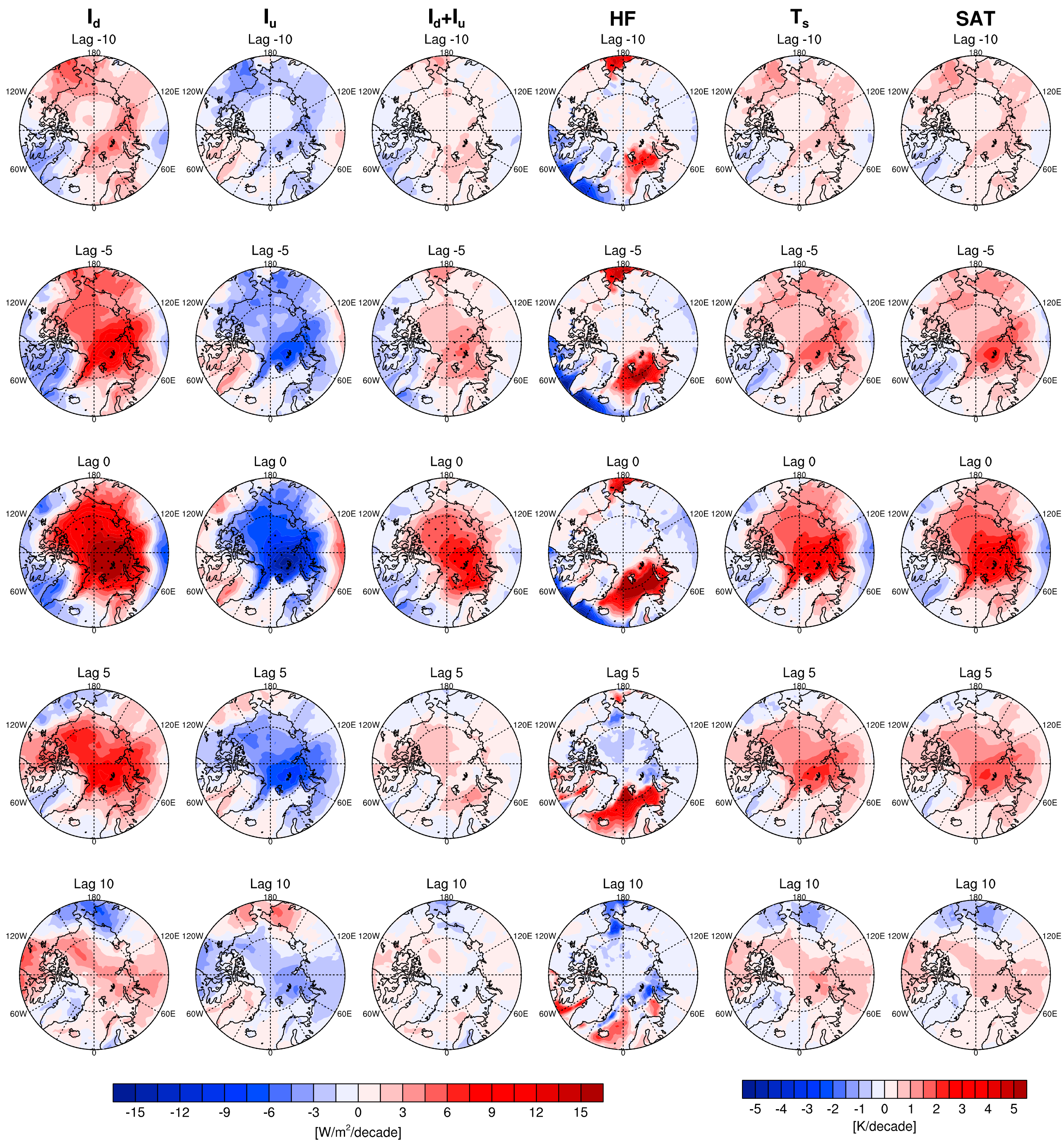

Figure 3. The trends obtained by multiplying the regression coefficients (regression against the IR index) and the trend in the IR index for different variables: the downward IR, upward IR, total IR, surface heat flux, skin temperature, and 2 m air temperature. The trends are shown from lag −6 day through lag 12.

the latent heat of vaporization, *L*) trend into the Arctic (Figure 2a). The region with the largest convergence occurs over the Greenland and Barents Seas where the surface heat flux trend is from the atmosphere to the surface (Figure 1c). Since the contribution to anomalies in downward IR by liquid water and ice is much greater than that by water vapor (E. Clothiaux, personal communication, 2017), we also calculate the trends in the total column-integrated ice and liquid water (Figure 2b) and downward IR (Figure 2c). As can be seen, the spatial pattern of the moisture flux convergence (multiplied by *L*) trend resembles that of both the total column liquid water plus ice and downward IR and has an amplitude of about one half that of the downward IR. These findings suggest that moisture fluxes from the midlatitudes into the Arctic are an important contributor to the downward IR trend poleward of 70°N.

As shown above (Figure 2), although moisture flux convergence is an important contributor to the downward IR trend, Figure 1d implies that an increase in evaporation could also be a substantial contributor to the downward IR trend over the Chukchi and Kara Seas. Integrating over the region north of 70 N, we find that the moisture flux convergence trend is 7.6×10^6 m^3 decade^{-1}, while the evaporation trend is much smaller and negative, -0.7×10^6 m^3 decade^{-1}. From this analysis, we conclude that averaged over the entire Arctic Ocean, moisture flux convergence played the dominant role in enhancing total column water accumulation over the cold season and thus downward IR.

3.3. Intraseasonal Evolution of the Surface Energy Budget

Given the evidence that the intraseasonal time scale circulation plays an important role in increasing the Arctic T_s (and SAT), it is insightful to examine the time evolution of the budget terms to gain a better understanding of the physical processes. Figure 3 shows $\Delta_x y(\tau)$ for various y and τ. It can be seen that downward IR ($\Delta_x I_d(\tau)$,first column) gradually increases from lag day -10 to day 0 and then declines afterward. The upward IR ($\Delta_x I_u(\tau)$, Figure 3 (second column)) pattern is almost identical to the downward IR pattern, except that for most lag days it is somewhat weaker; the total IR (downward minus upward) is positive for all lags throughout the Arctic except for lag +10 days (third column). The Arctic $\Delta_x T_s(\tau)$ and Δ_xSAT(τ) are positive, reaching their maximum values at $\tau = 0$. (These two fields are almost identical at all τ shown, again supporting the idea that budget equation (3) can be used to understand the SAT trend.) These results suggest that as warm moist air enters the Arctic (Figure 2a), downward IR first warms the surface, and in response, there is an increase in the upward IR emitted by the surface.

The surface heat flux (Figure 3, fourth column) adds to this picture: at negative lags, it is notably downward over the Greenland and most of the Barents Seas, indicating that there is anomalous heat transfer from the atmosphere to the surface in these seas. The downward flux builds up to lag zero ($\tau = 0$) and then declines. By lag +5 days for the Kara Sea, and lag +10 days for the Barents Sea, its sign changes and the surface heat flux is upward. We interpret these results to indicate that as warm moist air enters the Arctic, downward IR warms the surface (and melts sea ice where sea ice is present); as the intrusion event comes to an end, the surface heat flux turns upward.

4. Discussion and Conclusions

In this study, we revisited the analysis of SS10 by performing surface energy budget analysis. This investigation leads us to conclude that downward IR played the leading role in warming the Arctic over most of the Arctic Ocean for the same months (October–January) and years (1989–2009) as examined by SS10. We surmise that the overall discrepancy arises because in SS10 the net IR was compared to SAT. However, upon noting that the heat storage is negligible for a thin interface, and expressing the upward IR trend in terms of the skin temperature trend, the correct comparison is between the skin temperature trend (very similar to the SAT trend) and the downward IR trend, not the net IR trend, and the surface heat flux trends.

Over most of the Barents Sea, which may be regarded as a marginal sea ice zone, the surface heat flux trend is strongly downward, i.e., a turbulent heat transfer trend from the atmosphere to the ocean. The intraseasonal evolution of the surface fluxes reveals that the surface heat flux in this region changes sign and turns upward after downward IR heats the surface. Similar behavior was shown by Park, Lee, and Feldstein (2015), Woods and Caballero (2016), and Gong et al. (2017). Therefore, at least in this region and during the time period that we examined, the conventional picture that the surface warming is caused by turbulent heat flux from the ocean (be it the ice-albedo feedback during sunlit seasons or an enhanced influx of warm water from the North Atlantic) does not hold up.

Over the Chukchi, Laptev, and Kara Seas, the heat flux trend is upward, presumably reflecting the effect of declining sea ice cover and ice thickness. Especially over the Chukchi Sea and a small area of the Kara Sea, the upward heat flux trend is greater than the downward IR trend. This upward heat flux trend could be caused by ocean warming during the sunlit season when ice-albedo feedback can contribute to the warming. For the Chukchi Sea, this upward heat flux trend could also be caused by changes in the warm current from the Pacific Ocean (Peralta-Ferriz et al., 2014; Shimada et al., 2006).

It was shown that the downward IR trend is associated with a trend in the moisture fluxes from midlatitudes into the Arctic, as well as a trend in the total column liquid water and ice in the Arctic. Gong et al. (2017) showed that this moisture flux trend arises from a trend in synoptic time scale intrusions of moisture into the Arctic. Therefore, the results of this study imply that synoptic-scale moisture intrusion events, via their impact on downward IR, have a very large impact on the Arctic warming. However, over parts of the Chukchi and Kara Seas, where the surface heat flux trend is upward and with a larger magnitude than the downward IR trend, hence, it is possible that the positive SAT trend arises from an upward sensible and/or latent heat flux, as well as an increase in the downward IR due to the input of additional water vapor into the atmosphere. (Note that an upward sensible heat flux will, per se, reduce the skin temperature (cf. equation (2)). However, since the skin temperature trend (Figure 1a) and the SAT trend (SS10) both show a warming trend over the Chukchi and Kara Seas, the implication is that the skin temperature increase is due to conduction from below the surface and an increase in downward IR.) It is possible that in these two seas this process may dominate the impact of warm moist air intrusions. Further research with the horizontal sensible and latent heat flux convergence, together with radiative transfer calculations, should be able to clarify this issue.

Acknowledgments
The ERA-Interim data used in this study were downloaded from the ECMWF data server. This study was supported by National Science Foundation grants AGS-1455577and AGS-1401220 and the National Nature Scientific Foundation of China (41305048) and the National Basic Research Program of China (2012CB417403). Screen and Simmonds were supported by Australian Research Council grant DP160101997. We thank Rodrigo Caballero and an anonymous reviewer for their very helpful comments. There are no real or perceived financial conflicts of interests for any author. There are no other affiliations for any author that may be perceived as having a conflict of interest with respect to the results of this paper.

References

Baggett, C., Lee, S., & Feldstein, S. B. (2016). An investigation of the presence of atmospheric rivers over the North Pacific during planetary-scale wave life cycles and their role in Arctic warming. *Journal of the Atmospheric Sciences*, *73*, 4329–4347. https://doi.org/10.1175/JAS-D-16-0033.1

Chen, Y., Francis, J. A., & Miller, J. R. (2002). Surface temperature of the Arctic: Comparison of TOVS satellite retrievals with surface observations. *Journal of Climate*, *15*, 3698–3708.

Doyle, J. G., Lesins, G., Thackray, C. P., Perro, C., Nott, G. J., Duck, T. J., … Drummond, J. R. (2011). Water vapor intrusions into the High Arctic during winter. *Geophysical Research Letters*, *38*, L12806. https://doi.org/10.1029/2011GL047493

Gong, T., Feldstein, S. B., & Lee, S. (2017). The role of downward infrared radiation in the recent Arctic winter warming trend. *Journal of Climate*, *30*, 4937–4949. https://doi.org/10.1175/JCLI-D-16-0180.1

Gong, T., & Luo, D. (2017). Ural blocking as an amplifier of the Arctic sea ice decline in winter. *Journal of Climate*, *30*, 2639–2654. https://doi.org/10.1175/JCLI-D-16-0548.1

Lee, S., Gong, T., Johnson, N., Feldstein, S. B., & Pollard, D. (2011). On the possible link between tropical convection and the Northern Hemisphere Arctic surface air temperature change between 1958 and 2001. *Journal of Climate*, *25*, 4350–4367.

Lesins, G., Duck, T. J., & Drummond, J. R. (2012). Surface energy balance framework for Arctic amplification of climate change. *Journal of Climate*, *25*, 8277–8288.

Luo, B., Luo, D., Wu, L., Zhong, L., & Simmonds, I. (2017). Atmospheric circulation patterns which promote winter Arctic sea ice decline. *Environmental Research Letters*, *12*, 054017. https://doi.org/10.1088/1748-9326/aa69d0

Park, D.-S. R., Lee, S., & Feldstein, S. B. (2015). Attribution of the recent winter sea ice decline over the Atlantic sector of the Arctic Ocean. *Journal of Climate*, *28*, 4027–4033.

Park, H.-S., Lee, S., Son, S.-W., Feldstein, S. B., & Kosaka, Y. (2015). The impact of poleward moisture and sensible heat flux on Arctic winter sea ice variability. *Journal of Climate*, *28*, 5030–5040. https://doi.org/10.1175/%20JCLI-D-15-0074.1

Peralta-Ferriz, C., Morison, J. H., Wallace, J. M., Bonin, J., & Zhang, J. (2014). Arctic Ocean circulation patterns revealed by GRACE. *Journal of Climate*, *27*, 1445–1468. https://doi.org/10.1175/JCLI-D-13-00013.1

Screen, J. A., & Simmonds, I. (2010a). The central role of diminishing sea ice in recent Arctic temperature amplification. *Nature*, *464*, 1334–1337. https://doi.org/10.1038/nature09051

Screen, J. A., & Simmonds, I. (2010b). Increasing fall-winter energy loss from the Arctic Ocean and its role in Arctic temperature amplification. *Geophysical Research Letters*, *37*, L16707. https://doi.org/10.1029/2010GL044136

Serreze, M. C., Barrett, A. P., Stroeve, J. C., Kindig, D. N., & Holland, M. M. (2009). The emergence of surface-based Arctic amplification. *The Cryosphere*, *3*, 11–19.

Serreze, M. C., & Barry, R. G. (2011). Processes and impacts of Arctic amplification: A research synthesis. *Global and Planetary Change*, *77*, 85–96. https://doi.org/10.1016/j.gloplacha.2011.03.004

Serreze, M. C., & Francis, J. A. (2006). The Arctic amplification debate. *Climatic Change*, *76*, 241–264.

Shimada, K., Kamoshida, T., Itoh, M., Nishino, S., Carmack, E., McLaughlin, F., … Proshutinsky, A. (2006). Pacific Ocean inflow: Influence on catastrophic reduction of sea ice cover in the Arctic Ocean. *Geophysical Research Letters*, *33*, L08605. https://doi.org/10.1029/2005GL025624

Stroeve, J. C., Serreze, M. C., Holland, M. M., Kay, J. E., Maslanik, J., & Barrett, A. P. (2012). The Arctic's rapidly shrinking sea ice cover: A research synthesis. *Climatic Change*, *110*, 1005–1027. https://doi.org/10.1007/s10584-011-0101-1

Wallace, J., & Hobbs, P. (2006). *Atmospheric science: An introductory survey* (2nd ed.). Academic Press.

Woods, C., & Caballero, R. (2016). The role of moist intrusions in winter Arctic warming and sea ice decline. *Journal of Climate*, *29*, 4473–4485.

Woods, C., Caballero, R., & Svensson, G. (2013). Large-scale circulation associated with moisture intrusions into the Arctic during winter. *Geophysical Research Letters*, *40*, 4717–4721. https://doi.org/10.1002/grl.50912

Yoo, C., Lee, S., & Feldstein, S. B. (2012a). Arctic response to an MJO-like tropical heating in an idealized GCM. *Journal of the Atmospheric Sciences*, *69*, 2379–2393.

Yoo, C., Lee, S., & Feldstein, S. B. (2012b). Mechanisms of extratropical surface air temperature change in response to the Madden-Julian oscillation. *Journal of Climate*, *25*, 5777–5790.